Macromolecular Research, Vol. 10, No. 1, pp 24-33 (2002)

A study on the Interfacial Properties of Electrodeposited Single Carbon Fiber/Epoxy Composites Using Tensile and Compressive Fragmentation Tests

Joung-Man Park*

Department of Polymer Science & Engineering, Engineering Research Institute
Gyeongsang National University, Chinju 660-701, Korea

Jin-Won Kim

M-Biotech Inc., Salt Lake City, Utah, 84119, U.S.A

Received Nov. 10, 2001 ; Revised Dec. 19, 2001

Abstract : Interfacial and microfailure properties of carbon fiber/epoxy composites were evaluated using both tensile fragmentation and compressive Broutman tests. A monomeric and two polymeric coupling agents were applied via the electrodeposition (ED) and the dipping applications. A monomeric and a polymeric coupling agent showed significant and comparable improvements in interfacial shear strength (IFSS) compared to the untreated case under both tensile and compressive tests. Typical microfailure modes including cone-shaped fiber break, matrix cracking, and partial interlayer failure were observed under tension, whereas the diagonal slipped failure at both ends of the fractured fiber appeared under compression. Adsorption and shear displacement mechanisms at the interface were described in terms of electrical attraction and primary and secondary bonding forces.

Keywords : electrodeposition (ED), interfacial shear strength (IFSS), monomeric and polymeric coupling agents, tensile and compressive fragmentation Tests.

Introdution

Interfacial properties between fiber and matrix are very important to control the mechanical performance in composite materials. The single fiber pullout test[1] and single fiber composite (SFC) test (also known as fragmentation test),[2] have been commonly used to characterize the fiber-matrix interfacial properties of microcomposites in tension,[3,4] whereas the microindentation test was used in compression.[5] The single fiber pullout test (which is also known as microdroplet test)[1,3] can measure the IFSS by pulling out a fiber from a lump or microdroplet of the polymer matrix. In the microindentation test, a rigid indenter pushed in a cross-sectional head of the fiber in a thin plate of real composite. Single fiber pullout and microindentation tests are essentially similar with each other from the point of view that the IFSS can be determined directly by either pullout or push in a fiber. The SFC test, originally proposed by Kelly and Tyson[2] for metal matrix composite (MMC), can provide abundant statistical information as well as the microfailure modes and IFSS using several specimens.

Recently Ageorges *et al.*[6-8] investigated the single fiber Broutman test for the fiber-matrix interface with debonding and stress analysis by subjecting to a transverse tensile load with an aid of acoustic emission (AE). Marom *et al.*[9-11] studied the compressive fragmentation phenomena using microcomposites to evaluate thermal stresses, single carbon fiber compressive strength, Weibull parameter and their IFSS, as well as the strength-length dependence of carbon fiber. Transverse properties in the fiber-matrix interface were investigated by the single fiber Broutman test to know the interfacial debonding and buckling behavior while subjecting to a compressive stress.

IFSS can be improved by an introduction of chemical functional groups to the fiber surface via electrolytic oxidation,[12] ammonia plasma treatment[13] or coupling agent application.[14,15] Among them is the electrodeposition (ED),[16-18] which is a process that a film is deposited on a conductive carbon fiber from a dispersion of colloidal ions in aqueous solution with a charge opposite to that of the carbon fiber surface. By optimizing the treatment process, a polymeric coating can be deposited with the desired composition and thickness uniformly to improve the interfacial properties.

*e-mail : jmpark@nongae.gsnu.ac.kr

In this work, using a monomeric and two polymeric coupling agents, interfacial properties for the ED and the dipping treated carbon fiber/epoxy matrix composites were evaluated under either the tensile or compressive fragmentation tests. Microfailure modes were correlated with IFSS and adsorption mechanisms using coupling agents.

Experimental

Materials. Carbon fiber (Tae Kwang Co., TZ-307) has density of 1.8 g/cm^3 and average diameter of 7.9 μm, whereas tensile strength and modulus are 2883 and 245 GPa, respectively. One monomeric pyromellitic dianhydride (PMDA, Aldrich Chemical Inc.) and two polymeric coupling agents, polybutadiane-maleic anhydride (PBMA, Polyscience Inc.) and polystyrene-maleic anhydride (PSMA, Polyscience Inc.) were used for the ED and the dipping treatments on the carbon fiber surface. PSMA was partially soluble but the others were totally soluble in the deionized water. Chemical structures of one monomeric and two polymeric coupling agents are shown in Table I. Epoxy resin (YD-128, Kukdo Chemical Co., Korea) as matrix is based on diglycidylether of bisphenol-A (DGEBA), and polyoxypropylenediamine (Jeffamine D400, Huntsman Petrochemical Co.) was used as a curing agent. It was precured for 2 hrs at 80 °C and then postcured for 2 hrs at 120 °C. Tensile strength of used epoxy was 48.1 MPa and modulus was 2.19 GPa whereas elongation to failure was 5.7% and yield strength was about 30 MPa. The untreated basalt fiber (Washington State University Laboratory, Pullman, WA) with 97 μm in diameter was also used only for the comparison of different size effect.

Methodologies.

Single Fiber Strength Measurement, Fiber Surface Treatment and Microspecimen Preparation: Tensile strength of single carbon fiber was obtained using about fifty specimens for statistical meaningful value. Average diameter of fifty fibers was measured via an optical microscope equipped with a calibrated eyepiece. Single fibers were placed in the centerline on the middle of each paper frame. The fiber was fixed using Scotch tape, and then finally glued the fiber using an epoxy adhesive. Universal testing machine (UTM) (LR-10K, Lloyd Instrument Ltd., U.K.) was used to measure the single fiber tensile strength. Load cell of 100 N was used and the crosshead speed was 0.5 mm/minute.

Three coupling agents were diluted to 0.5 wt% concentration in deionized aqueous solution. Carbon fiber was modified via either the ED or the dipping treatments for the comparison. The carbon fibers acted as an anode by themselves whereas the cathode was composed of an aluminum plate as shown in Figure 1. After the anode frame and the cathode bar

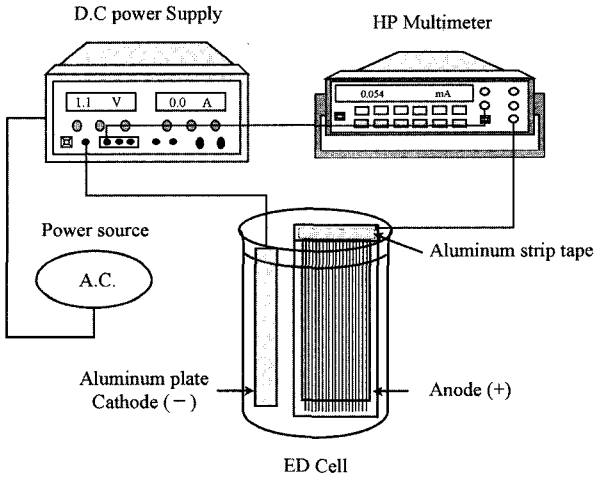

Figure 1. Schematic plot of ED system.

Table I. Chemical Structures of a Monomeric and Two Polymeric Coupling Agents

Type	Chemical Name	Chemical Structure
Monomeric	Pyromellitic Dianhydride (PMDA)[a]	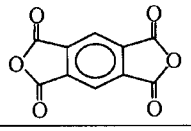
Polymeric	Polybutadiene-Maleic anhydride (PBMA)[b]	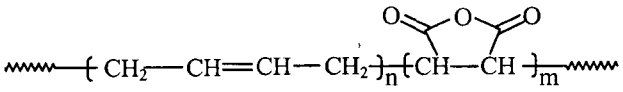
	Polystyrene-Maleic anhydride (PSMA)[b]	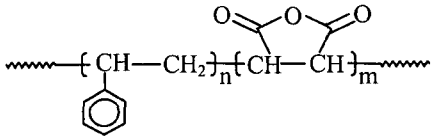

[a]Aldrich Chemical Inc.
[b]Polyscience Inc.
*m and n are constant.

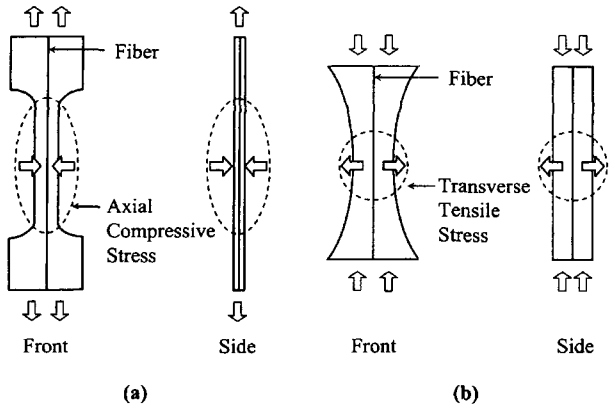

Figure 2. Schematic illustration showing the dimension of two-type specimens for (a) tensile dogbone-shaped specimen; and (b) compressive curved neck Broutman specimen.

were immersed into certain electrolyte solution, constant voltage was applied to both electrodes by a conventional DC regulated power supply (GP 4303TP, LG Electronics, Korea) and corresponding current was recorded using a multimeter (HP 34401A) plus personal computer (PC) as shown in Figure 1. From the previous work,[18] typical immersing time and applied voltage were set as 10 minutes and 3 voltages, respectively. Dipping was performed for 2 minutes in the same aqueous solution as ED treatment. Tensile and compressive microspecimens were made of single fiber embedded in epoxy matrix in different silicone moulds as shown in Figure 2. Dogbone-shaped tensile specimen was made for conventional fragmentation test, whereas compressive specimen was made as curved neck shape, where a fiber is laid down longitudinally in two different mould. After pouring epoxy resin, they cured together in the same oven in order to provide identical conditions.

Tensile and Compressive IFSS Measurements: To determine tensile IFSS the ultimate fiber fragment lengths were measured individually, and subsequent failure process was observed via a polarized-light microscope with a calibrated eyepiece. Tensile specimens were tested by UTM with 10 kN load cell and crosshead speed rate of 0.25 mm/minute. On the other hand, the compressive test was performed with same 10 kN load cell and a crosshead speed of 2 mm/minute for carbon fiber composite and 1 mm/minute for basalt fiber composite. The relationship among fiber tensile strength, σ_f, aspect ratio l_c/d, and tensile IFSS, τ_t was given originally by Kelly-Tyson equation[2] as

$$\tau_t = \frac{\sigma_{f,ut} \cdot d}{2l_c} \tag{1}$$

where $\sigma_{f,ut}$ is the fiber tensile strength at average critical length, l_c, and d is the fiber diameter.

According to Wood *et al.*,[9,10] under compression the original stress profile along the fiber could be almost unchanged by the fiber fracture. Because as the first approximation the compressive stress might assume to be transferred perfectly across the fiber break region from one fiber fragment to another. As the compressive stress on the fiber increased further, the fiber might break again at a stress level corresponding to larger compressive strength of new smaller fragment in accordance with the strength-length dependence called as Weibull weakest link rule. Appling compressive stress on the specimen might not result in an increase in the stress on the fiber and hence the critical fragment length might consider being the same as an original length. Unlike in the conventional tensile fragmentation test, the average fragment length might be unrelated to a critical fragment length. The compressive shear stress can be calculated from the compressive stress in the matrix as approximated by von Mises criterion[6] as

$$\tau_c = \frac{\sigma_m}{\sqrt{3}} \tag{2}$$

where σ_m is the matrix stress being equal in the matrix and in the fiber, and it can be obtained as

$$\sigma_m = \sigma_{f,ut}(l)\frac{E_m}{E_f} \tag{3}$$

where $\sigma_{f,uc}(l)$ is the compressive strength at length, l, and E_m and E_f are the Young's moduli of the matrix and the fiber, respectively. It may be unnecessary to know the fiber stress transfer length, l_T.

Figure 3 shows schematic diagrams of stress profile with increasing stress under (a) tension and (b) compression. In Figure 3(a), Kelly-Tyson model assumes that the tensile stress in the fiber builds up from the broken fiber ends and that the fragmentation occurs when the built stress in the fiber reaches the fiber tensile strength. As tensile stress is applied further, the fiber fracture process continues until no longer fracture occurred in the fiber. At this strain a fragment length is called as a critical fragment length, l_c. The critical fragment length of the individual fiber was measured and their microfailure modes were observed via a polarized-light microscope. In compressive test in Figure 3(b), unlike in tensile test, the fiber fragmentation does not result in a stress discontinuity at fiber fracture point, because the fiber fragments remain in contact and can still bear compressive load, i.e., the stress state around the center region of the original fiber remains constant and equal to the compressive stress on the fiber.[6]

As another view on compressive IFSS by Oshawa *et al.*,[19] compressive IFSS, τ_c can be also based on the force balance as,

$$\tau_c = \frac{\sigma_{f,uc}(l_c)_{comp}d}{2(l_c)_{comp}} \tag{4}$$

where $\sigma_{f,uc}$ is the compressive strength of the fiber at critical fragment length, l_c at pure shear region around center of

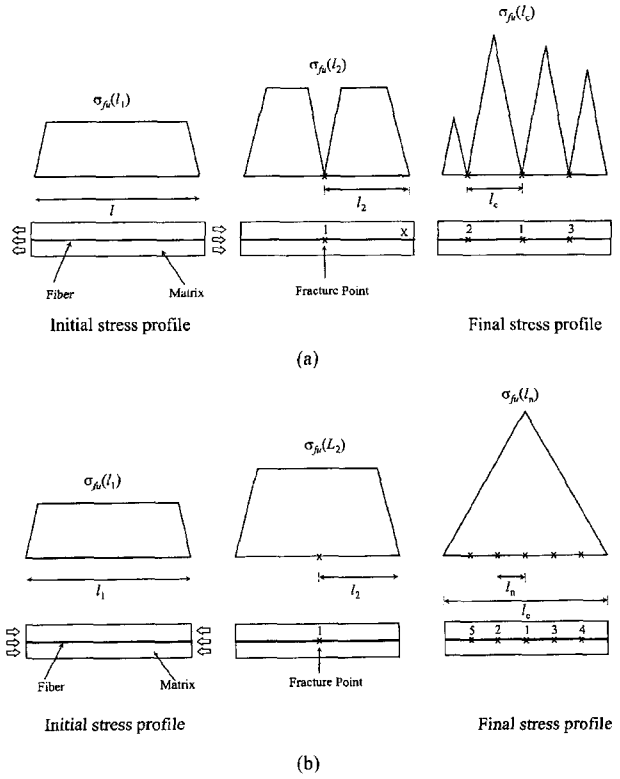

Figure 3. Schematic diagram of stress profile with increasing loading under (a) tension and (b) compression.

the specimen, and d is the fiber diameter. $\sigma_{f,uc}$ is the fiber compressive stress at the state where the interfacial stress is insufficient to induce further fragmentation. The fragment length in compression was considered to relate to the critical length in tension in the same way in Eq. (1), with substituting only compressive indexes. Making the assumption that the IFSS under either tension or compression are equal, the compressive strength of the fiber was simply defined by

$$\frac{\sigma_{f,uc}}{\sigma_{f,ut}} = \frac{(l_c)_{comp}}{(l_c)_{tension}} \tag{5}$$

Fiber strength can be calculated from the extrapolated gauge length using Weibull weakest link rule.[20,21] The fiber strength, σ_f at the critical fragment length is

$$\sigma_f = \sigma f_0 \cdot \left(\frac{l_c}{l_0}\right)^{-\frac{1}{\beta}} \tag{6}$$

where σ_{f0} is fiber strength at gauge length, l_0 and l_c is average fragment length, and β is shape parameter of the Weibull distribution of the fiber strength.

Results and Discussion

Tensile and Compressive Tensile Strength of Modified Carbon Fiber. Table II shows the properties of the tensile strengths for the untreated and the treated carbon fibers. Tensile strength of the treated carbon fiber was significantly improved with respect to that of the untreated fibers, showing a similar value for both the ED and the dipping treatments. Direct measurements of the compressive strength of carbon fiber present the experimental difficulty. According to Wagner *et al.*,[11] carbon fiber is known to get compressive strength to tensile strength ratios of only 10-30% for a high moduli type exhibiting in the range of 380-480 GPa, where compressive strength is remarkably low. However, the ratio of the compressive strength to tensile strength for a low modulus carbon fiber in the range of 260 GPa by the transverse tensile test was found to be 66.4%. According to Oshawa,[19] the ratio of compressive strength to tensile strength is approximately a half under the hypothesis of stress continuity at the break point. In this work, compressive strength of carbon fiber to the measured tensile strength was calculated from Eq. (5) by Oshawa.

In addition, for the difference in the fiber strength between tension and compression, it might be due to the anisotropic properties based on the molecular and structural differences of carbon fiber between axial and transverse

Table II. The Properties of the Tensile Strengths for the Untreated and the Treated Carbon Fibers

Types		No. of Specimen (EA)	Diameter (μm)	Scale Parameter (α)	Shape Parameter (β)	Tensile Strength (MPa)[b]
Untreated		49	7.9 (0.1)[a]	3098	6.08	2883 (534)
ED	PMDA	50	8.1 (0.1)	3375	5.39	3424 (627)
	PBMA	44	8.9 (0.3)	3483	5.44	3606 (615)
	PSMA	46	8.1 (0.1)	2321	5.92	2896 (704)
DP	PMDA	42	8.0 (0.1)	3239	5.41	3363 (655)
	PBMA	43	8.2 (0.3)	3434	5.53	3684 (583)
	PSMA	39	8.2 (0.1)	3256	6.31	3498 (532)

[a]Parenthesis is standard deviation (SD).
[b]Gauge length of specimen: 20 mm.

directions, i.e., strong covalent bonding may act on the axial direction under tension, whereas rather weak hydrogen or secondary bonding can act on the transverse direction under compression. Tensile strength of carbon fiber by the ED and the dipping method showed a significant improvement, due to the healing effect of the fiber flaw working as stress concentration in addition to enhanced wetting effect. The reason for less improvement of tensile strength for PSMA treatment than the dipping method might be because of intensely compact packing on the carbon fiber surface with ionized electrolytes.

Comparison of Compressive and Tensile Microfailure Modes. As originally proposed by Broutman,[22] the curved-neck specimen under compression causes the interfacial debonding to occur in the transverse direction. Applied compressive stress results in the largest transverse tensile stress at the narrowest center portion of the curved-neck specimen. Tensile debonding occurs due to the transverse expansion of the matrix when Poissons ratio of matrix is greater than that of the fiber. Since Poissons ratio of the matrix is larger than that of the fiber, the transverse expansion of the matrix is also larger than that of the fiber and a transverse debonding stress can be induced at the interface. This thermal expansion mismatch causes to a transverse debonding stress at the interface. Debonding starts to occur in the middle of the specimen where the transverse stress is the maximum.[6,7]

In the case of good interfacial bonding, the fiber may fail first under compressive stress before any interface damage can start. Single fiber compressive test has not been so much popular as tensile microcomposite test because of the experimental difficulties in preparing the specimen and in detecting the onset of the interfacial de-bonding visually as well as in determining IFSS. In order to obtain reproducible results, single fiber should be aligned accurately and precisely.

Figure 4 shows the photographs of microfailure modes for carbon fiber/epoxy composites under tensile test. In Figure 4(a), the untreated carbon fiber fracture under tension occurred with the debonding and low degree of stress whitening phenomena appeared around a fiber fracture point. In Figure 4(b), ED treated carbon fiber occurs cone-shaped fracture mode and high degree of stress whitening phenomena was observed at two points of fractured carbon fiber. In Figure 4(c), the dipping treated carbon fiber exhibited the debonding with moderate degree of stress whitening. It might be due to reduced interfacial adhesion between carbon fiber and epoxy.

Figure 5 shows photographs of microfailure modes for carbon fiber/epoxy composites under compressive test. The diagonal slippage of carbon fiber fracture in compression appeared based on the transverse tensile stress. Stress whitening phenomena was also observed around fiber slippage, and the failure modes of the ED treated case appeared rather sharp edge in the slipped end compared to either the

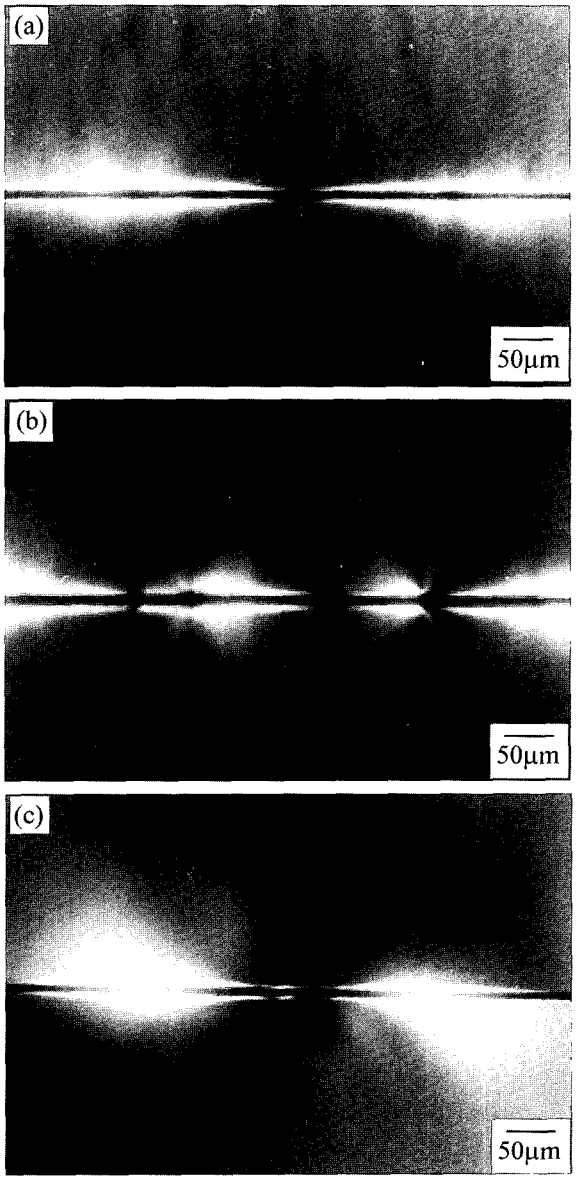

Figure 4. Polarized-light photographs showing the microfailure modes for (a) the untreated, (b) ED treated, and (c) the dipping treated carbon fiber under tensile tests.

untreated or the dipping cases, respectively. Figure 6 shows photographs of failed shape of basalt fiber composites under (a) tension and (b) compression. Figures (a) and (b) can show the magnified failure modes and stress whitening distribution around a fracture point of basalt fiber more clearly. The difference between tension and compression may be due to much larger 98 μm in diameter compared to 7.9 μm carbon fiber. However, general failure trends were similar to each other.

In Figure 7, simplified model of the fracture modes for carbon fiber is shown for (a) before stress applied, (b) under tension and (c) under compression. It shows the different

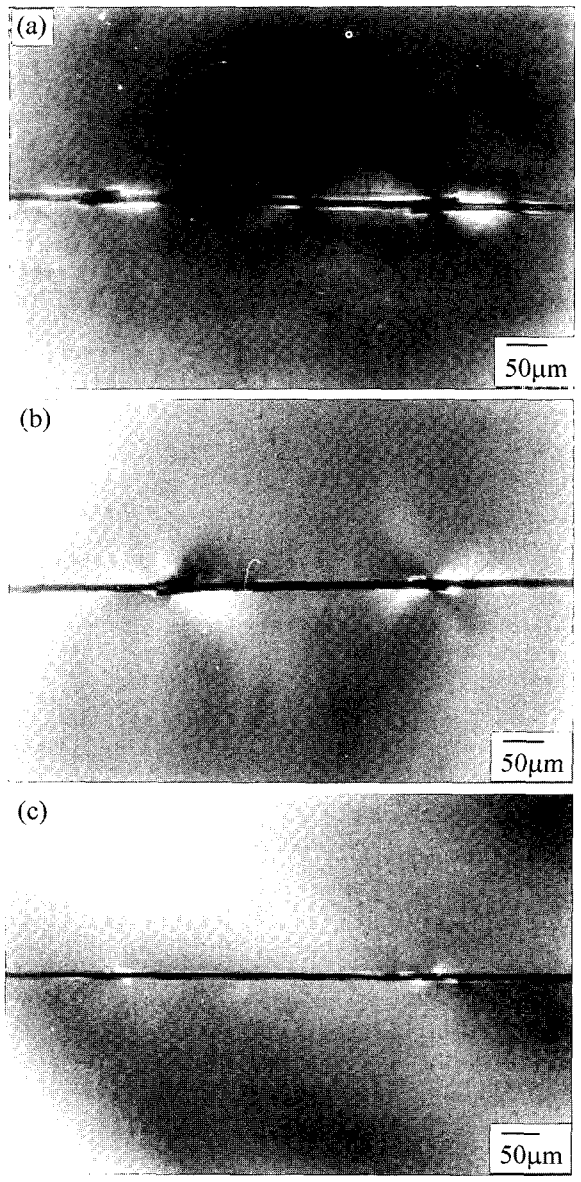

Figure 5. Polarized-light photograph showing the microfailure modes for (a) the untreated, (b) ED treated, and (c) the dipping treated carbon fiber under compressive tests.

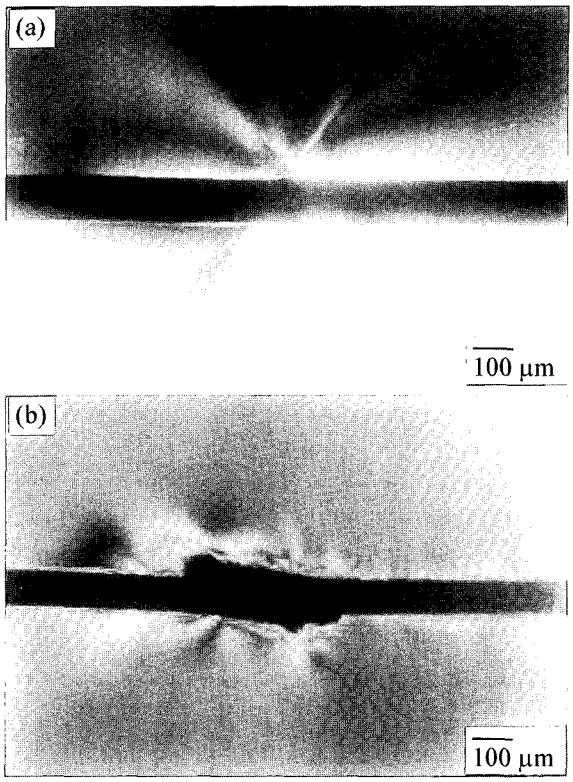

Figure 6. Photographs of microfailure modes of basalt fiber under (a) tension and (b) compression.

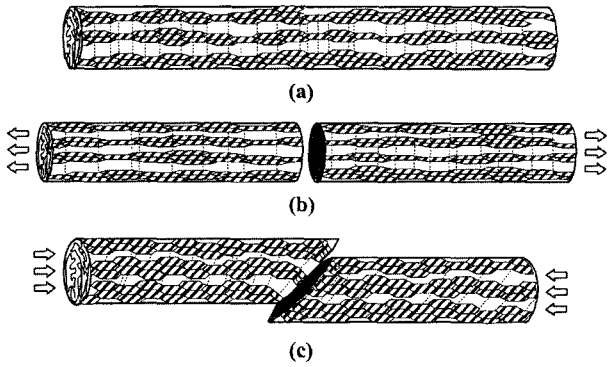

Figure 7. Scheme of fracture modeling of carbon fiber under tensile and compressive loadings.

molecular failure mechanisms between tension and compression. Under tensile loading the fracture of carbon fiber occurred due to the breakage of strong C-C covalent bonding, whereas under compression carbon fiber exhi-bited kink band failure across the whole fiber length. It was due to the failure of the secondary bonding and the simple shear deformation against the initial compressive stress and then the fiber fracture progressed toward the kink slip plane.

Comparison of Tensile and Compressive IFSS. In compression, the fragments at the fiber fracture points remain in contact and thus the normal stress at the fiber ends is not zero. Wood *et al.*[9,10] assumed that since there was no stress discontinuity at the fracture points, the stress state over the fiber fragment length remained constant and equal to the compressive stress in the fiber in Figure 3(b). This assumption may not be true when the birefringence pattern is observed due to a discontinuity of the stress at fiber fracture points. In addition, the final slipped shape indicates that the fractured plane is not perpendicular to the fiber but declined with an angle, which would affect the stress transfer from one fragment to another. Nevertheless, under this assumption the fragmentation process is dependent upon the compressive

Table III. Aspect Ratio and IFSS Improvement for ED and the Dipping Applications under Tensile and Compressive Tests

	Type		Aspect Ratio (l_c/d)	Critical Fragment Length (l_c) (μm)	Fiber Strength (MPa)[a]		IFSS (MPa)	Improv. (%)
Tensile	Untreated		72.9	576	5167		35.4[d]	-
	ED	PMDA	56.6	458	6898		59.4	68
		PBMA	52.5	462	7208		61.6	74
		PSMA	60.3	488	5422		43.8	24
	DP	PMDA	66.8	534	6569		48.6	37
		PBMA	61.4	503	7169		56.2	59
		PSMA	70.9	581	6128		41.6	17
Comp.	Untreated		36.2	286	2879[b]	1682[c]	8.6[e]	-
	ED	PMDA	30.6	247	4180	2221	11.4	34
		PBMA	28.9	245	4305	2296	11.7	39
		PSMA	32.2	261	3219	1825	9.3	9
	DP	PMDA	34.6	277	3843	2088	10.7	26
		PBMA	30.3	248	4020	2171	11.1	31
		PSMA	30.6	251	3021	1764	9.0	5

[a]Tensile fiber strengths, $\sigma_{f,ut}$ at critical fragment length, l_c.
[b]Compressive fiber strengths, $\sigma_{f,uc}$ at critical fragment length, l_c.
[c]Compressive fiber strengths, $\sigma_{f,uc}$ at critical fragment length, l_c at average fragment range of 75 mm.
[d]Tensile IFSS obtained by Kelly-Tyson method, Eq. (1).
[e]Compressive IFSS obtained by Wood method, Eq. (2).

strength with the fragment length and not upon the shear stress transfer from the matrix to fiber. According to Wood *et al.*, this aspect of the compressive fragmentation test may be an advantage over tensile fragmentation, since it is unnecessary to know the critical load transferring length from matrix to fiber for the determination of the IFSS.

The measurement of the compressive strength of a single fiber is experimentally difficult, and no method has been currently standardized.[23] Several methods have been used to estimate the compressive fiber strength including the technique with which the fiber is tested in air without surrounding any matrix. In the embedded case, the results are affected by the factors such as matrix type and modulus, the interfacial adhesion plus specimen preparation, etc. Oshawa *et al.*[19] determined the compressive strength from the fiber fragment length in the compressive fragmentation test. They assumed that the stress transfer mechanism in the tensile fragmentation might be also valid in compressive fragmentation; i.e., the normal stress at the fiber fragment end is zero.

Table III shows the aspect ratio and IFSS and their improvement for ED and the dipping applications under tensile and compressive tests. IFSS by either ED or the dipping applications showed a high improvement compared to the untreated case under both tension and compression. Since IFSS is a function of aspect ratio and fiber strength at a critical fragment length, tensile fiber strength value, l_c was obtained using Weibull weakest link rule by extrapolating the measurable fiber strength at a critical fragment length. Compressive tensile strength at a critical fragment length was about 60% range values with respect to tensile strength at the critical fragment length. Interfacial debonded failure under compressive stress was determined by well-known von Mises criterion relating to shear yielding of the epoxy matrix. On the other hand, compressive IFSS determined by Oshawa method was reasonably similar to tensile IFSS, which means the upper limit. The difference between two methods comes from mainly the concept of fibers stress discontinuity and other parameters. Not unexpectedly, compressive IFSS appeared lower than tensile IFSS according to Wood method. Compressive IFSS might be even lower than shear yield strength of the currently used epoxy matrix, about 30 MPa at 25 °C.

Figure 8 shows that a monomeric, PMDA and a polymeric, PBMA coupling agents exhibited significant and comparable improvement in IFSS with respect to the untreated case under both tensile and compressive tests. It is ascribed to the primary and the secondary chemical bonding as well as physical interdiffusion at the possible interface between coupling agents and epoxy matrix. In the tensile test the ED treated specimen exhibited higher IFSS improvement than the dipping case. Better wetting due to polymeric nature and more uniform coating contribute to IFSS favorably. On the other hand, the compressive test shows the comparative IFSS improvement for the ED and the dipping

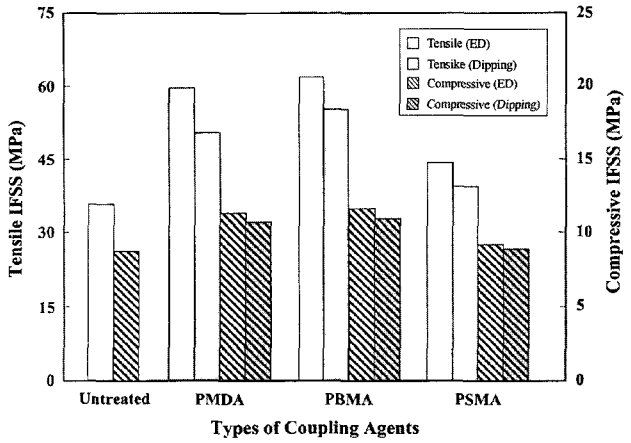

Figure 8. IFSS for three coupling agents with respect to the untreated case.

applications unlike the tensile test despite the different failure mechanisms between tension and compression. In case of the enhanced interfacial bonding by coupling agents, more number of fibers failed under compressive stress prior to the interfacial debonding occurred and then progressed. In addition, the difference in IFSS between the tension and the compression is also ascribable to different molecular displacements while fracture process is going on. PSMA showed much less improvement in IFSS compared to either monomeric PMDA or same polymeric PBMA, especially in tension, possibly because of the interlayer deposited with less uniformity. However, the IFSS of PSMA was also significantly higher than the untreated case for all cases.

In general, two competitive microfailure mechanisms may appear in compressive Broutman test, i.e., the fiber fracture under compressive stress *versus* transverse debonding of fiber-matrix interface.[6] First, in case of the strong interfacial bonding, the fiber fracture may occur in advance. It is because the compressive stress subjecting to the composite exceeds the fiber compressive strength prior to transverse debonding stress exceeds the interfacial transverse strength. The result reflects the shear properties at the interface with more fiber fragments in the ED case. Second, when the interfacial transverse strength is not so strong, the interfacial debonding under compressive stress occurs first. The result can be characteristic transverse properties at the interface with less number of fiber fracture and severe debonding length.

Figure 9 shows a schematic model of possible bonding mechanisms among carbon fiber, either (a) monomeric or (b) polymeric coupling agents and epoxy matrix. In the first interphase between carbon fiber surfaces and coupling agents, there may be both the primary chemical bonding and the secondary hydrogen bonding. In the secondary interphase between coupling agent and epoxy matrix chemical bonding and the interdiffusion may contribute to improve the interfacial adhesion further.

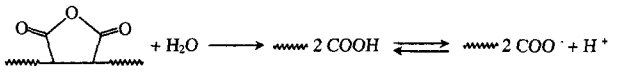

(7)

Anhydride groups attached to either monomeric or polymeric coupling agents can be hydrolyzed in aqueous solution to offer carboxylic groups after anhydride ring opening reaction occurs in Eq. (7). Anhydride group reacts with minor functional group in the carbon fiber surface, such as ether, hydroxyl, and carboxyl groups etc. With carboxylate groups, the anodic oxidation may result in the crosslinking of coupling agents by themselves, or the grafting of the coupling agents onto the carbon fiber. The reactions may result in the improved interfacial adhesion and then enhanced the mechanical performance of composite materials under tension and compression. Epoxy resin mixed with amine curing agents can react with coupling agent treated carbon fiber. The reorientation of coupling agent molecules around carbon fiber and epoxy matrix can occur. Plueddemann[24] proposed simplified model of the shear displacement in Figure 10. If a

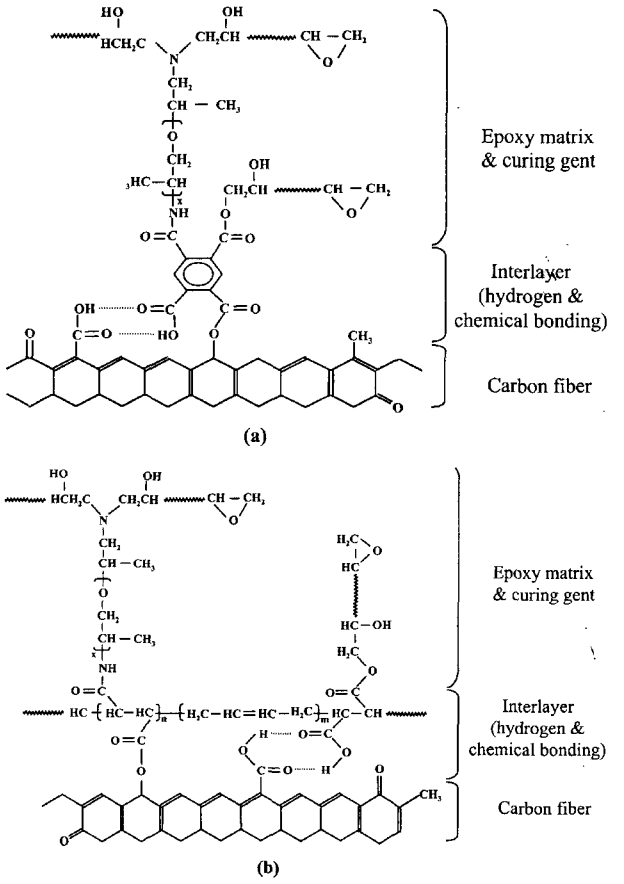

Figure 9. Possible illustration for chemical reaction among carbon fiber, epoxy matrix and either (a) monomeric PMDA or (b) polymeric PBMA coupling agents.

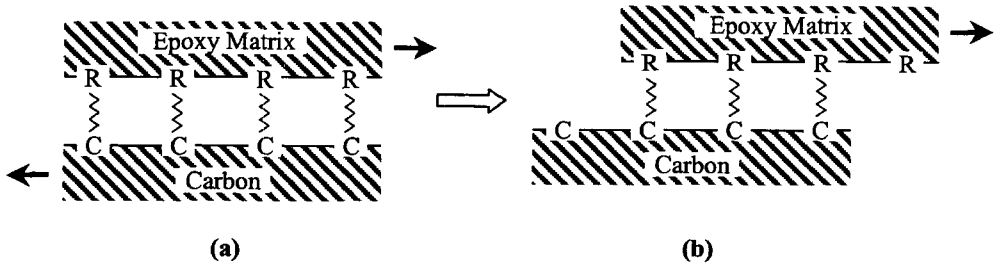

Figure 10. Shear displacement at the interface without permanent bond rupture.

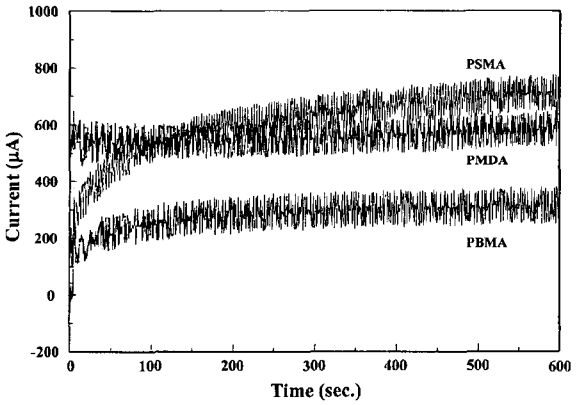

Figure 11. Current changes during ED process with three different coupling agents.

Table IV. Current and pH Changes in Coupling Agent Solution during ED Process

Type	Chemical Name	pH	Current (μA)		
			10 sec.[a]	300 sec.	600 sec.
Monomeric	PMDA[b]	2.11	560	540	560
Polymeric	PBMA	2.68	170	290	310
	PSMA	2.67	250	640	720

[a]ED time.
[b]Concentration of coupling agent: 0.5 wt%.

shear stress occurs parallel to the interface, the fiber and matrix can glide past each other without permanent bond rupture due to the dynamic equilibrium of chemical reaction under either tension or compression.

Figure 11 and Table IV show the typical current and their pH changes during ED processing in PMDA solution. In case of monomeric PMDA, the maximum current reached in a short time and then showed a steady state. It might be due to small molecular size to move easily in aqueous solution. Initially the current of a polymeric PSMA increased rapidly and then reached a steady state, whereas another polymeric PBMA showed a similar trend except that the current level was relatively low. In the monomeric PMDA, low molecular movement can be active and the concentration of electrolytes

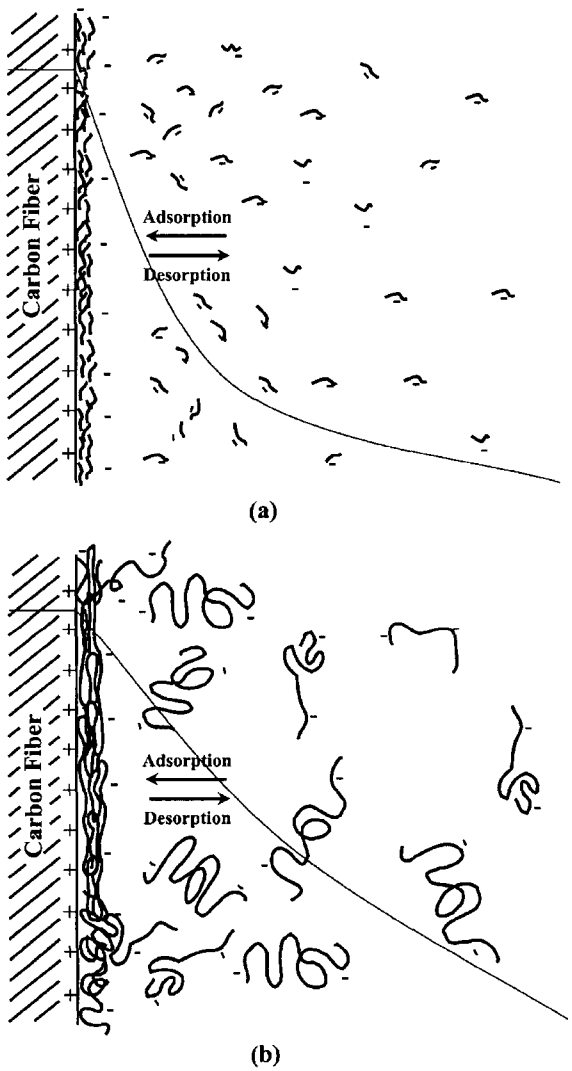

Figure 12. Schematic illustrations of adsorption and desorption mechanisms in the electrolyte solution using (a) monomeric and (b) polymeric coupling agents.

in aqueous solution is high at the beginning. However, as adsorption process went on further, the current level decayed slightly. On the other hand, the number of electrolytic ions of polymeric chain might be rather smaller than the

number of monomeric ions. For polymeric PSMA the current increased continuously with elapsing adsorption time, and IFSS value was low since an excessively adsorbed interlayer on the fiber acts as a defect like the stress concentration, resulting in the deterioration of the interfacial adhesion.

Figure 12 shows schematic mechanisms of the adsorption and desorption between carbon fiber surfaces for dissolved (a) monomeric and (b) polymeric coupling agents in acidic aqueous solution. Equilibrium state between the adsorption and desorption might occur. Excessively adsorbed coupling agents are dissolved again especially at elevated temperature and provide high concentrated electrolytes near the fiber surface.[14,18] During ED processing the adsorption of coupling agent can occur mainly due to the electrical attraction by the polarization of the electrolytes and carbon fiber surface in aqueous solution. As ED process goes on, however, electrical attraction force diminishes and instead of it another secondary bonding, such as van der Waals force acts on the interphase between carbon fiber and adsorbed coupling agent. In Figure 12(a), monomeric coupling agent exhibited the rapid drop of the electrolyte density from the carbon fiber surface due to smaller mole-cular size. On the other hand, in Figure 12(b), electrolyte density decreased steadily with increasing the distance from the fiber surface in polymeric coupling agent. It is due to the larger molecular size and their steric effect. Simplified model in Figure 12 is consistent with the current change result with elapsing time in Figure 11.

Conclusions

With tensile fragmentation and compressive Broutman tests, interfacial properties including IFSS and microfailure mechanisms were investigated using one monomeric and two polymeric coupling agents via ED and the dipping applications. A monomeric and one polymeric coupling agent exhibited significant and comparable improvements in IFSS with respect to the untreated case under both tensile and compressive tests. In tension, ED treated composites showed higher IFSS than the dipping application, exhibiting cone- shape fiber fracture due to the compact and uniformly deposited interlayer. In compression, however, there was less difference in IFSS between ED and the dipping. And diagonal slippage based on the transverse tensile stress at the interface was observed in compression test. Basalt fiber composite with large diameter exhibited significantly distinct failure modes, especially in compression. Adsorption and shear displacement mechanisms at the interface could be due to electrical attraction and primary and secondary bonding forces in aqueous solution, which contributed to analyze the tensile and compressive IFSS.

Acknowledgement. This study was financially supported from CAMP of the 21th C Frontier R&D Program funded by the Ministry of Science and Technology, Korea through Engineering Research Institute (ERI), Gyeongsang National University.

References

(1) T. Grubb, and Z. F. Li, *J. Mater. Sci.*, **29**, 189 (1994).
(2) A. Kelly and W. R. Tyson, *Mech. and Phys. of Solids*, **13**, 329 (1965).
(3) J. M. Park, S. I. Lee, D. W. Shin, and D. J. Yoon, *Polym. Compos.*, **20**, 19 (1999).
(4) J. M. Park, W. G. Shin, and D. J. Yoon, *Compos. Sci. Technol.*, **59**, 355 (1999).
(5) D. B. Marshall and W. C. Oliver, *Mater. Sci. Eng.*, **A 126**, 95 (1990).
(6) C. Ageorges, K. Friedrich, and L. Ye, *Compos. Sci. Technol.*, **59**, 2101 (1999).
(7) C. Ageorges, K. Friedrich, T. Schuller, and B. Lauke, *Composites: Part A*, **30**, 1423 (1999).
(8) T. Schuller, W. Beckert, B. Lauke, C. Ageorges, and K. Friedrich, *Composites: Part A*, **31**, 661 (2000).
(9) J. R. Wood, H. D. Wagner, and G. Marom, *Proc. Royal Soc. London. A*, **452**, 235 (1996).
(10) J. R. Wood and G. Marom, *Appl. Compos. Mater.*, **4**, 117 (1997).
(11) H. D. Wagner, C. Migliaresi, A. H. Gilbert, and G. Marom, *J. Mater. Sci.*, **27**, 4175 (1992).
(12) C. M. Ballie and M. G. Bader, *J. Mater. Sci.*, **29**, 3822 (1994).
(13) Z. F. Li, A. N. Netravali, and W. Sachse, *J. Mater. Sci.*, **27**, 4625 (1992).
(14) J. M. Park, *J. Colloid Interf. Sci.*, **225**, 384 (2000).
(15) J. M. Park, J. O. Lee, and C. W. Park, *Polym. Compos.*, **17**, 375 (1996).
(16) R. V. Subramanian and A. S. Crasto, *Polym. Compos.*, **7**, 201 (1986).
(17) J. M. Park, Y. M. Kim, K. W. Kim, and D. J. Yoon, *Proceedings of ICCE/6*, Orlando, U.S.A., 1999, pp 645-646.
(18) J. M. Park, Y. M. Kim, K. W. Kim, and D. J. Yoon, *J. Colloid Interf. Sci.*, **231(1)**, 114 (2000).
(19) T. Oshawa, M. Miwa, and M. Kawade, *J. Appl. Polym. Sci.*, **55**, 1733 (1990).
(20) H. F. Wu and A. N. Netravali, *J. Mater. Sci.*, **27**, 3318 (1992).
(21) K. Goda, J. M. Park, and A. N. Netravali, *J. Mater. Sci.*, **30**, 2722 (1995).
(22) L. T. Broutman, *ASTM STP* **452**: American Society for Testing Materials, 1969, pp 27-41.
(23) R. N. Singh, *J. Am. Ceram. Soc.*, **73**, 2930 (1990).
(24) E. P. Plueddemann, in *Interface in Polymer Matrix Composites*, Academic Press, New York, 1974, pp 174.